

Pattern formation in ferrogels: analysis of the Rosensweig instability using the energy method

Stefan Bohlius¹, Harald Pleiner¹ and Helmut R Brand²

¹ Max Planck Institute for Polymer Research, 55021 Mainz, Germany

² Theoretische Physik III, Universität Bayreuth, 95440 Bayreuth, Germany

E-mail: pleiner@mpip-mainz.mpg.de

Received 15 May 2006, in final form 20 July 2006

Published 8 September 2006

Online at stacks.iop.org/JPhysCM/18/S2671

Abstract

We present a nonlinear description of the Rosensweig instability in isotropic magnetic gels based on the energy minimizing method used by Gailitis to describe the Rosensweig instability in typical ferrofluids. We extend his discussion to media with elastic degrees of freedom, assuming the shear modulus as a perturbation to the pure fluid case. We study the relative stability of the regular planforms of stripes, squares and hexagons as a function of the elastic shear modulus.

1. Introduction

1.1. Ferrofluid convection

Ferrofluids are suspensions of magnetic nanoparticles in a suitable carrier liquid. They are coated by polymers or charged in order to prevent coagulation. They show various distinct material properties, like superparamagnetism (large magnetic susceptibility, high saturation magnetization in rather low fields), sensitivity to magnetic Kelvin forces, and a rather complicated influence of magnetic fields on their flow behaviour [1, 2]. This has led to numerous important applications as seals (in hard disk drives), active dampers (clutches), thermal conductors (loudspeakers), as well as in the medical sector (hyperthermia, drug targeting in cancer therapy). The favourable ferrofluid properties are generally preserved when dealing with more complex systems, like ferronematics and ferrogels. In addition, new features are coming into play, leading to quite unusual and novel types of behaviour. Ferronematics are obtained if the carrier liquid is a lyotropic or thermotropic nematic liquid crystal, while ferrogels are produced by combining polymers and ferrofluids and crosslinking them into a gel [3]. If the latter process is performed in an external field, a uniaxial ferrogel with a frozen-in magnetization is obtained [4]. We are interested in the unconventional macroscopic dynamic behaviour of typical ferrofluids and, in particular, in the unusual behaviour of unconventional ‘ferrofluids’, i.e. materials using ferrofluids as ingredients such as ferronematics and ferrogels.

Viewed as binary mixtures of magnetic particles and a carrier fluid, ferrofluids have rather extreme properties. With the grain size being large on molecular length scales, the

particle mobility (or concentration diffusivity) is extremely small (very small Lewis number L), allowing us to disregard the concentration dynamics in most cases [5, 6]. However, this simplification does not hold for thermal convection since, due to the pronounced Soret effect of these materials in combination with a considerable solutal expansion (large separation ratio ψ), the resulting solutal buoyancy forces are dominant. By considering the classical Rayleigh Bénard setup, it has been shown [7] that both the linear as well as the nonlinear convective behaviour is significantly altered by the concentration field as compared to single-component systems. Starting from an initial motionless configuration with a uniform concentration distribution, convective perturbations are found to grow even at Rayleigh numbers well below the threshold Ra_c^0 of pure-fluid convection. It turns out that the actual critical Rayleigh number Ra_c is drastically smaller but experimentally inaccessible due to the extremely slow growth of convection patterns for $Ra \gtrsim Ra_c$, requiring extremely large observation times. On the other hand, operating the ferrofluid convection experiment at Rayleigh numbers $Ra_c < Ra \lesssim Ra_c^0$ reveals considerable positive growth rates, which lead to a saturated nonlinear state almost as fast as pure-fluid convection does at $Ra > Ra_c^0$.

In an external magnetic field the apparent imperfection of the bifurcation is even more pronounced. Magnetophoretic effects, as well as magnetic stresses, have been taken into account in the static and dynamic parts of the equations, leading to rather pronounced boundary layer profiles (with respect to the concentration and magnetic potential). This boundary layer couples effectively to the bulk behaviour due to the magnetic boundary conditions [8].

Another interesting case is ferrofluids with a negative separation ratio (negative Soret coefficient). When heating from below molecular binary mixtures with a negative separation ratio, the thermal and solutal density gradients are opposite to each other, such that the linear stationary thermal instability is suppressed for $\psi < -1$. Instead, this antagonistic behaviour leads to a linear convective instability of oscillatory type at Ra_c^0 , the critical Rayleigh number for the onset of convection in the single fluid case. This feature is also found for ferrofluids, but the nonlinear treatment shows that the linearly unstable oscillatory states are transients only and decay after some time, rendering the final convection-free state stable [9]. Above a second threshold, somewhat higher than Ra_c^0 , a finite amplitude stationary instability is found, while small amplitude disturbances do not destroy the convection-free state. If molecular binary mixtures with a separation ratio $\psi < -1$ are heated from above, a linear stationary instability is found, which is basically driven by the solutal buoyancy and only slightly modified by thermal variations. In ferrofluids, however, this stationary instability is very different from that obtained by heating from below with a positive separation ratio, since the concentration and temperature dynamics show completely different behaviour. In the former case, small-scale structures arise at very high Ra numbers, whose wavelength decreases strongly with increasing Ra . For smaller Ra numbers ($|Ra| \sim Ra_c^0$) the procedure of using the separation of thermal conduction and concentration diffusion times breaks down.

In the nonlinear domain the question of pattern formation and competition has been discussed numerically and using model amplitude equations for ferrofluids with positive and negative separation ratios [10].

1.2. Ferronematics

If the carrier liquid is a nematic liquid crystal, several phases are possible. Using a Landau-type free-energy function, one can describe the phase transitions from an isotropic (superparamagnetic) ferrofluid to a ferromagnetic nematic liquid crystal either directly or via a superparamagnetic nematic liquid crystal [11]. These two nematic phases are usually both called ‘ferronematic’, although they are distinct phases. Both show nematic ordering, but only

the ferromagnetic phase shows spontaneous magnetic ordering, additionally. In the presence of a strong external magnetic field, these transitions are smeared out and the different ferronematic phases become rather similar to each other. In nature, no ferromagnetic ferronematic phase has been found until today, so the theoretical macroscopic considerations have been restricted to the superparamagnetic variant.

In equilibrium, the orientation of the nematic director and of the magnetization (induced by an external magnetic field) are locked. The macroscopic dynamics of ferronematics can be described on two different levels, either assuming the magnetization to be relaxed to its static value, or it can be treated as an additional dynamic (slowly relaxing) degree of freedom. In the former case, the equations are structurally the same as for an ordinary nematic liquid crystal, except for the fact that the influence of the magnetic field is much more intense. However, in ordinary nematics, linear magnetic field effects in the dynamics have never been discussed or detected, possibly due to their smallness. In ferronematics, there is a good chance to find those effects, which arise as various linear field (Hall-like) contributions to the fluxes [12]. These new dynamic effects predicted come in four classes. First, the alignment of the nematic director in shear flow is modified by an external field such that the director has a component out of the shear plane, even if the field is in the shear plane. Second, the heat flux due to a temperature gradient, in a magnetic field orthogonal to the latter, induces an additional reversible heat current that is perpendicular to both. Third, a linear field contribution to viscosity leads, for a magnetic field orthogonal to the propagation direction of a sound wave, to a force on a tracer particle in the third direction. Fourth, when the director is reoriented in an external magnetic field, its relaxation is accompanied by an oscillation that is not observed in usual nematics.

Another possibility for probing the dynamic linear field contributions is the detection of their qualitatively new effects on some well-known instabilities [13]. In the Rayleigh–Bénard instability with the temperature gradient opposite to gravity, one gets, in addition to convection flow in the form of one-dimensional rolls, a vorticity flow. As a consequence, in the homeotropic case (the director oriented parallel to the magnetic field) the streamlines are oblique to the roll cross-section, while in the planar case (the director perpendicular to the magnetic field, but parallel to an electric field) the rolls themselves are tilted with respect to the director, depending on the magnetic field strength. In the Saffman–Taylor viscous fingering instability of a growing interface between fluids of different density, the new linear magnetic-field contributions lead to a rotation of the finger structure.

The complete set of macroscopic dynamic equations for ferronematics includes the magnetization as an independent slowly relaxing variable [14]. Orientational changes of the magnetization are coupled to nematic director reorientations not only in the statics, but in the dynamics as well. In addition, there are reversible and dissipative dynamic crosscouplings between (compressional, shear and elongational) flow, (rotations and changes of the absolute value of the) magnetization and director reorientations. Some of these couplings are only possible when an external magnetic field is present. Some combinations of the parameters that describe these crosscouplings can be measured by employing sound waves and shear rheology. For a sound wave propagating in a direction oblique to the preferred directions (equilibrium magnetization, nematic director), compressional flow (and changes of the absolute value of the magnetization) are coupled to shear flow (and rotations of the director and the magnetization). There is also a field-dependent contribution to sound damping. In addition, the linear response of the system to oscillatory shear flow has been discussed, concentrating on frequencies below the transverse magnetization relaxation frequency. This shows directly the influence of the magnetic dynamic degree of freedom on the director dynamics. Even without a magnetic field, the modified nematic director diffusion couples to the flow. As a consequence, the apparent viscosity is different from the bare one. In the presence of an external field, the director

diffusion/relaxation is shifted to a finite frequency, which increases approximately with the third power of the field strength.

1.3. Ferrogels

Due to the crosslinking in ferrogels, a network is created that gives rise to elasticity. The truly hydrodynamic variable describing elasticity is the displacement field, or more appropriately for nonlinear theories, the strain tensor. Isotropic ferrogels are superparamagnetic and the magnetization is an additional independent slowly relaxing variable, which allows us to study the system for rather high frequencies as well [15]. The fact that magnetic grains are attached to the network is expressed by the static coupling of the magnetization and the strain tensor (magnetostriction). This leads to an additional field-dependent contribution to the sound spectrum. The contribution to the transverse sound modes depends on the relative angle between an external field and the wavevector. From the low frequency limit of the sound spectrum, one can obtain information about the effective magnetic-field-dependent elastic moduli. However, these moduli are different from those measured by static elongations or shear deformations in an external field. The reason is that, due to the finite magnetostriction, the linear response theory is not applicable. Only in the limit of a vanishing field are they equal and matching the true elastic moduli. In the high-frequency limit, one gets a shift in the sound velocities proportional to the dynamic coupling between the flow and the magnetization. This reflects the fact that the magnetization is an independent variable. Finally, we proposed that, in an experiment with an oscillating temperature gradient as well as a gradient of the magnetic field, shear waves are excited [15].

Ferromagnetic gels are uniaxial if the frozen-in magnetization denotes the only preferred direction. Such materials are potentially very interesting for a variety of applications. Uniaxial magnetic gels show, on the one hand, similarities to other anisotropic gels, like nematic elastomers, and to isotropic ferrofluids and ferrogels, but the combination of preferred direction, magnetic degree of freedom, and elasticity makes them unique and very unusual. Prominent features are [16] the relative rotations between the magnetization and the elastic network, which couple dynamically flow, shear, and magnetic reorientation. As a result, shear flow in a plane that contains the frozen-in magnetization induces a rotation of the magnetization, not only within the shear plane but also out of the shear plane. This behaviour is qualitatively different from that of other types of materials. The basic results hold, even if the constant shear flow is replaced by an oscillating one, which is very likely in actual experiments, although the formulae for that case will become much more complicated. Another outstanding aspect of the hydrodynamics of this material is the difference between the mass current density (mass density times velocity) and the momentum density due to a non-vanishing magnetization vorticity. Unheard of in other classical condensed phases, this is known from some uniaxial quantum fluids, where, however, experiments on this aspect are currently out of reach. In uniaxial ferromagnetic gels, the static susceptibilities for momentum fluctuations (the long-wavelength limit of the static momentum correlation functions) are given by the (bare) mass density for some geometries only, but show an increased renormalized effective density for other directions. In addition, an oscillating external magnetic field induces not only an oscillation of the magnetization in the direction of the external field, but also oscillating shear strains. The latter are found in planes that contain the frozen-in magnetization and either the external field or the third, perpendicular direction. In addition, the external field also induces a magnetization component perpendicular to both the field and the frozen-in magnetization. The reversible transport coefficient that governs this effect can be calculated by referring to the microscopic quantum mechanical spin-type dynamics for magnetic moments and using

the projector formalism to evaluate the frequency matrix. This coefficient vanishes with the magnetization and is, thus, characteristic for this type of ferromagnetic gel.

Surface undulations of the free surface of viscous liquids are known to be able to propagate as gravity or capillary waves. In more complex systems like viscoelastic liquids or gels, the transient or permanent elasticity allows for modified transverse elastic waves at free surfaces [17]. They are excited, e.g. by thermal fluctuations or by imposed temperature patterns on the surface. In ferrofluids, magnetic stresses at the surface come into play. In particular, in an external magnetic field normal to the surface, there is a focusing effect on the magnetization at the wave crests of an undulating surface with the tendency to increase the amplitude of the undulations [1]. Above a critical field strength, wave propagation is not possible anymore and the surface becomes unstable with respect to a stationary pattern of surface spikes (Rosensweig or normal field instability). The same linear instability mechanism is operative when dealing with (isotropic) ferrogels where elasticity comes into play as an additional stabilizing factor. Using linearized dynamic equations and appropriate boundary conditions, one gets [18] the general surface wave dispersion relation for ferrogels (in a normal external field), which contains, as special cases, those for ferrofluids and non-magnetic gels and can be generalized to viscoelastic ferrofluids and magnetorheological fluids. A linear stability analysis reveals the threshold condition, above which stationary surface spikes grow. This critical field depends on gravity, surface tension and on the elastic (shear) modulus of the gel, while the critical wavelength of the emerging spike pattern is independent of the elastic modulus of the gel. As in the case of ferrofluids, neither the threshold nor the critical wavelength depends on the viscosity.

A linear theory can determine neither the actual spike pattern nor the true nature of the instability (forward, backward etc). The standard weakly nonlinear (amplitude expansion) theory that provides suitable amplitude equations, by which these questions can be answered, is more complicated in the present situation due to two problems. First, the driving force of the instability is manifested in the boundary conditions but not in the bulk equations, and second the surface profile (the location where the boundary conditions have to be applied) changes with the order of the amplitude expansion. Thus, for ferrofluids a different path has been chosen [19, 20]. Neglecting the viscosity (and any other dissipative process) from the beginning, the system is Hamiltonian and its stability is governed by a free energy, more precisely by the surface free energy, since the magnetic destabilization acts at the surface. We generalize this approach to (isotropic) ferrogels by taking into account in addition the elastic free energy. The results have to be taken with the caveat that neglecting the viscosity is justified at the (linear) instability threshold, but is an unproven assumption for the nonlinear domain and for the pattern formation and selection processes.

2. Surface energy density

Describing typical ferrofluids within the framework of the energy minimization method, the expression for the energy density at the surface was first given by Gailitis [19]. Assuming an incompressible ferrofluid occupying the negative half-space, the surface energy density has three contributions: a gravitational term accounting for the hydrostatic energy; a contribution due to surface tension; and the energetic contribution of the magnetic field that is applied perpendicular to the initially flat surface. Averaging the entire surface, one obtains [19] as the difference in energy density with respect to the flat configuration

$$\mathcal{U}(\xi) = \frac{1}{2} \rho g \langle \xi^2(x, y) \rangle + \sigma \left\langle \sqrt{1 + (\text{grad } \xi(x, y))^2} \right\rangle + \frac{1}{2\mu_0\mu} \left\langle \int_{-\infty}^{+\infty} B^2(x, y, z) dz \right\rangle. \quad (1)$$

In our notation, the surface deflection from its unperturbed flat state is described by $\xi(x, y)$ and the magnetic induction by \mathbf{B} . The surface energy density depends on the mass density ρ , the gravitational acceleration g , the surface tension σ and the magnetic permeability of the vacuum μ_0 and the medium μ . Averaging with respect to the surface S is understood in the following usual way:

$$\langle F(x, y) \rangle = \lim_{S \rightarrow \infty} \frac{1}{S} \int \int_S F(x, y) dx dy. \quad (2)$$

For the surface deflection itself, we take a superposition of different wavevectors that can be divided into two groups. The first group will contain all those vectors whose wavelength corresponds to the critical one. The second group accounts for all the possible higher harmonic wavevectors, constructed from the main modes via superposition with Fourier modes in space (\mathbf{k}) and time (ω):

$$\xi(x, y, t) = \sum_{i=1}^M A_{\mathbf{k}_i} \cos(\mathbf{k}_i \cdot \mathbf{r}) e^{i\omega t} + \sum_{\substack{i,j=1 \\ \mathbf{k}_i \pm \mathbf{k}_j \neq 0}}^N A_{\mathbf{k}_i \pm \mathbf{k}_j} \cos((\mathbf{k}_i \pm \mathbf{k}_j) \cdot \mathbf{r}) e^{i\omega t}. \quad (3)$$

In this ansatz, we already assume regular two-dimensional patterns.

Starting to describe elastic media with this method, we have to account for the elastic degrees of freedom. This may be done by just adding an additional energetic contribution due to elastic deformations (described by the strain field ϵ_{ij}) to the surface energy density (1), as given by Jarkova *et al* [15]:

$$\left\langle \int_{-\infty}^{\xi} \frac{1}{2} \mu_{ijkl} \epsilon_{ij} \epsilon_{kl} dz \right\rangle. \quad (4)$$

It is sufficient to take the integral with respect to z just from the bottom ($-\infty$) to the top (ξ) of the ferrogel, since we assume vacuum in the positive half-space [18]. The explicit form of the elastic tensor μ_{ijkl} was given by Jarkova *et al* [15] and takes the following form in an incompressible medium, with μ_2 being the elastic shear modulus:

$$\mu_{ijkl} = \mu_2 (\delta_{ik} \delta_{jl} + \delta_{il} \delta_{jk}). \quad (5)$$

In total, we therefore get the following expression for the surface energy density in an incompressible, isotropic ferrofluid that is now left for minimization with respect to different regular patterns arising at the gel–vacuum interface beyond the linear threshold:

$$\begin{aligned} \mathcal{U}(\xi) = & \left\langle \frac{\rho g}{2} \xi^2 + \sigma \sqrt{1 + (\partial_x \xi)^2 + (\partial_y \xi)^2} + \frac{1}{2\mu_0 \mu} \int_{-\infty}^{+\infty} B^2(x, y, z) dz \right. \\ & \left. + 2\mu_2 \int_{-\infty}^{\xi} (\epsilon_{xy}^2 + \epsilon_{yz}^2 + \epsilon_{xz}^2) dz + \mu_2 \int_{-\infty}^{\xi} (\epsilon_{xx}^2 + \epsilon_{yy}^2 + \epsilon_{zz}^2) dz \right\rangle. \quad (6) \end{aligned}$$

In order to minimize equation (6) with respect to the amplitudes of the surface deflection, we first have to find the explicit expressions for the strain field in terms of $\xi(x, y, t)$. We therefore solve the system of equations given in [18], where we introduced a scalar potential ϕ and a vector potential Ψ for the different contributions of the velocity, namely $\mathbf{v}^{\text{pot}} = \nabla \phi$ and $\mathbf{v}^{\text{rot}} = \nabla \times \Psi$. To fulfill the tangential boundary conditions at the surface, these potentials have to be of the form

$$\hat{\Psi}_x = -\frac{2k(-ik_y)}{q^2 + k^2} \hat{\phi} \quad \text{and} \quad \hat{\Psi}_y = +\frac{2k(-ik_x)}{q^2 + k^2} \hat{\phi} \quad (7)$$

$$\hat{\phi} = i\omega \frac{q^2 + k^2}{k(q^2 - k^2)}. \quad (8)$$

We recall the fact that there appeared a different decay-length $2\pi/q$ with respect to the z -direction for the components of the vector potential Ψ , where

$$q^2 = k^2 - \frac{\rho\omega^2}{\mu_2 - i\omega\nu_2}, \quad (9)$$

with k being the absolute value of \mathbf{k} and ν_2 the shear viscosity.

Since dissipation will not play a role in the minimization of the energy density for this stationary instability, we discard the viscosity in equation (9) for the rest of our discussion. Following the ansatz given in [18], the explicit expressions for the three components of the velocity field eventually take the form

$$v_x = \sum_i (-ik_{ix}) \left(e^{k_i z} - 2 \frac{q_i k_i}{q_i^2 + k_i^2} e^{q_i z} \right) \frac{i\omega(q_i^2 + k_i^2)}{k_i(q_i^2 - k_i^2)} \xi_i \quad (10)$$

$$v_y = \sum_i (-ik_{iy}) \left(e^{k_i z} - 2 \frac{q_i k_i}{q_i^2 + k_i^2} e^{q_i z} \right) \frac{i\omega(q_i^2 + k_i^2)}{k_i(q_i^2 - k_i^2)} \xi_i \quad (11)$$

$$v_z = \sum_i k_i \left(e^{k_i z} - 2 \frac{k_i^2}{q_i^2 + k_i^2} e^{q_i z} \right) \frac{i\omega(q_i^2 + k_i^2)}{k_i(q_i^2 - k_i^2)} \xi_i, \quad (12)$$

where the sum is understood to account for all possible wavevectors under consideration, the main modes as well as the higher harmonic modes.

With the assumptions made in [18], the strain is dynamically coupled to the velocity field \mathbf{v} via

$$\partial_t \epsilon_{ij} = \frac{1}{2} (\nabla_i v_j + \nabla_j v_i). \quad (13)$$

Substituting equations (10)–(12) into (13), we find for the different components of the strain tensor, again as a sum with respect to all possible wavevectors under consideration,

$$\epsilon_{zz} = \sum_i \frac{(q_i^2 + k_i^2)e^{k_i z} - 2q_i k_i e^{q_i z}}{q_i^2 - k_i^2} k_i \xi_i \quad (14)$$

$$\epsilon_{xz} = \sum_i (-ik_{ix}) (e^{k_i z} - e^{q_i z}) \frac{q_i^2 + k_i^2}{q_i^2 - k_i^2} \xi_i \quad (15)$$

$$\epsilon_{yz} = \sum_i (-ik_{iy}) (e^{k_i z} - e^{q_i z}) \frac{q_i^2 + k_i^2}{q_i^2 - k_i^2} \xi_i \quad (16)$$

$$\epsilon_{xy} = - \sum_i k_{ix} k_{iy} \frac{q_i^2 + k_i^2}{k_i(q_i^2 - k_i^2)} \left(e^{k_i z} - 2 \frac{q_i k_i}{q_i^2 + k_i^2} e^{q_i z} \right) \xi_i \quad (17)$$

$$\epsilon_{xx} = - \sum_i k_{ix}^2 \frac{q_i^2 + k_i^2}{k_i(q_i^2 - k_i^2)} \left(e^{k_i z} - 2 \frac{q_i k_i}{q_i^2 + k_i^2} e^{q_i z} \right) \xi_i \quad (18)$$

$$\epsilon_{yy} = - \sum_i k_{iy}^2 \frac{q_i^2 + k_i^2}{k_i(q_i^2 - k_i^2)} \left(e^{k_i z} - 2 \frac{q_i k_i}{q_i^2 + k_i^2} e^{q_i z} \right) \xi_i. \quad (19)$$

In the limit of a stationary instability ($\omega \rightarrow 0$), we then obtain the following expressions:

$$v_i = 0 \quad (20)$$

$$\epsilon_{zz} = - \sum_i k_i^2 z e^{k_i z} \xi_i (\omega = 0) \quad (21)$$

$$\epsilon_{xz} = - \sum_i (-ik_{ix}) k_i z e^{k_i z} \xi_i (\omega = 0) \quad (22)$$

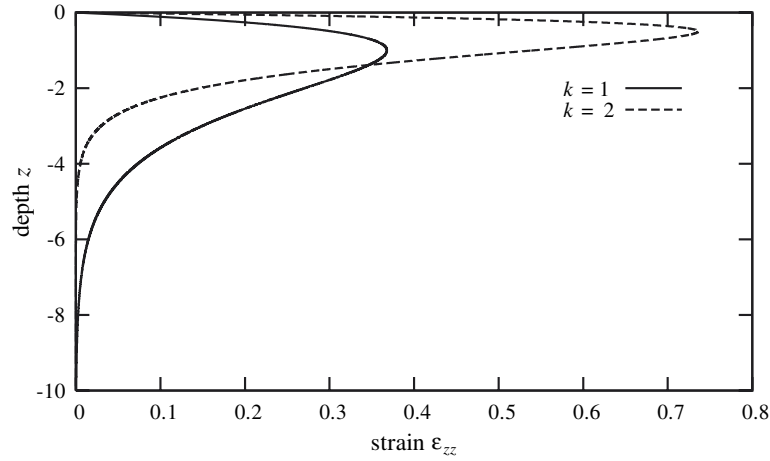


Figure 1. Absolute value of the strain for two particular modes, $k = 1$ and 2 respectively, according to (21) as a function of depth and for an arbitrary infinitesimal deflection of the surface at a given point (x, y) .

$$\epsilon_{yz} = - \sum_i (-ik_{iy})k_{iz}e^{k_iz}\xi_i(\omega = 0) \quad (23)$$

$$\epsilon_{xy} = \sum_i k_{ix}k_{iy}ze^{k_iz}\xi_i(\omega = 0) \quad (24)$$

$$\epsilon_{xx} = \sum_i k_{ix}^2ze^{k_iz}\xi_i(\omega = 0) \quad (25)$$

$$\epsilon_{yy} = \sum_i k_{iy}^2ze^{k_iz}\xi_i(\omega = 0). \quad (26)$$

The limit $\omega \rightarrow 0$ can only be performed after ϵ_{ij} has been calculated, due to equation (13). In figure 1 the decay of the strain field ϵ_{zz} along the z -axis is plotted for two different wavevectors in dimensionless units. These are chosen such that lengths are measured in units of the inverse characteristic wavevector $k_c^{-1} = \sqrt{\sigma/\rho g}$, energy densities in terms of σ , the magnetic field in units of the critical magnetic field, and the elastic shear modulus μ_2 in terms of $\sqrt{\sigma\rho g}$.

Using expressions (21)–(26) we can now formulate the final expression for the surface energy density. The nonelastic parts—represented by the first three terms in equation (6)—are taken from the discussions of Gailitis [19], because they do not change in the presence of elasticity. The fourth and fifth contribution in equation (6) are integrated and lead to the expression for the energy density up to fourth order of the amplitude A of the surface deflection $\xi(x, y)$:

$$\begin{aligned} \mathcal{U} = & -\frac{1}{2}\mathcal{E}(B_0, 1) \sum_{i=1}^N A_{\mathbf{k}_i}^2 + \frac{\mu_2}{2} \sum_{i=1}^N \mathcal{C}(\mathbf{k}_i) A_{\mathbf{k}_i}^2 \\ & - \mathcal{Q}(2\pi/3) \sum_{\substack{i,j,l \leq N \\ \mathbf{k}_i \pm \mathbf{k}_j \pm \mathbf{k}_l}} A_{\mathbf{k}_i} A_{\mathbf{k}_j} A_{\mathbf{k}_l} + \frac{1}{4}\mathcal{K}(0) \sum_{i=1}^N A_{\mathbf{k}_i}^4 \\ & + \sum_{i,j \leq N} \mathcal{K}(\Theta_{ij}) A_{\mathbf{k}_i}^2 A_{\mathbf{k}_j}^2 \end{aligned}$$

$$\begin{aligned}
& -\frac{1}{2} \sum_{i=1}^N \left(\mathcal{Q}(0) A_{\mathbf{k}_i}^2 A_{2\mathbf{k}_i} + (\mathcal{E}(B_0, 2) - \mu_2 \mathcal{C}(2\mathbf{k}_i)) A_{2\mathbf{k}_i}^2 \right) \\
& - \sum_{\pm} \sum_{\substack{i < j \leq N \\ |\mathbf{k}_i \pm \mathbf{k}_j| \neq 1}} \left(\mathcal{Q}(\pi/4 \pm \Theta_{ij} \mp \pi/4) A_{\mathbf{k}_i} A_{\mathbf{k}_j} A_{\mathbf{k}_i \pm \mathbf{k}_j} \right. \\
& \left. + \frac{1}{2} (\mathcal{E}(B_0, |\mathbf{k}_i \pm \mathbf{k}_j|) - \mu_2 \mathcal{C}(\mathbf{k}_i \pm \mathbf{k}_j)) A_{\mathbf{k}_i \pm \mathbf{k}_j}^2 \right) \\
& + \mathcal{O}(A^5). \tag{27}
\end{aligned}$$

The analytical coefficients of the non-elastic contributions in equation (27) have been given already by Gailitis [19]. For completeness, they are repeated here. The elastic coefficients follow from averaging equation (6) and are given here as functions of the components of the different wavevectors:

$$\mathcal{E}(B_0, k) = \epsilon k - \frac{1}{2} (1 - k)^2 \tag{28}$$

$$\begin{aligned}
\mathcal{K}(\Theta) &= \sin^3(\Theta/2) + \cos^3(\Theta/2) - \frac{9}{16} - \frac{1}{8} \cos(\Theta) \\
&+ \eta^2 (2 - \sin(\Theta/2) - \cos(\Theta/2)) \\
&- \sin^3(\Theta/2) - \cos^3(\Theta/2) \tag{29}
\end{aligned}$$

$$\mathcal{Q}(\Theta) = \eta (2 \cos(\Theta/2) - \cos^2(\Theta/2)) \tag{30}$$

$$\mathcal{C}(\mathbf{k}_i) = \frac{k_{ix}^2 k_{iy}^2}{2k_i^3} + \frac{k_{ix}^2}{2k_i} + \frac{k_{iy}^2}{2k_i} + \frac{k_{ix}^4}{4k_i^3} + \frac{k_{iy}^4}{4k_i^3} + \frac{k_i^4}{4k_i^3} \tag{31}$$

with $\eta = \chi/(2 + \chi)$.

As a first step to minimize expression (27), we note that all contributions with higher harmonics are—similarly to the case of usual ferrofluids—of the form

$$\mathcal{Q}(\pi/4 \pm \Theta_{ij} \mp \pi/4) A_{\mathbf{k}_i \pm \mathbf{k}_j} - \frac{1}{2} (\mathcal{E}(B_0, |\mathbf{k}_i \pm \mathbf{k}_j|) - \mu_2 \mathcal{C}(\mathbf{k}_i \pm \mathbf{k}_j)) A_{\mathbf{k}_i \pm \mathbf{k}_j}^2. \tag{32}$$

Minimizing separately with respect to these higher harmonic amplitudes, we find

$$A_{\mathbf{k}_i \pm \mathbf{k}_j} = \frac{\mathcal{Q}(\pi/4 \pm \Theta_{ij} \mp \pi/4)}{\mathcal{E}(B_0, |\mathbf{k}_i \pm \mathbf{k}_j|) - \mu_2 \mathcal{C}(\mathbf{k}_i \pm \mathbf{k}_j)}. \tag{33}$$

Substitution into equation (27) leads to the final form of the surface energy density as a function of the basic mode amplitudes:

$$\begin{aligned}
\mathcal{U} &= -\frac{1}{2} \sum_{i=1}^N (\mathcal{E}(B_0, |\mathbf{k}_i|) - \mu_2 \mathcal{C}(\mathbf{k}_i)) A_{\mathbf{k}_i}^2 \\
&- \mathcal{Q}(2\pi/3) \sum_{\substack{i, j, l \leq N \\ \mathbf{k}_i \pm \mathbf{k}_j \pm \mathbf{k}_l = 0}} A_{\mathbf{k}_i} A_{\mathbf{k}_j} A_{\mathbf{k}_l} \\
&+ \frac{1}{4} \sum_{i=1}^N \left(\mathcal{K}(0) + \frac{1}{2} \frac{\mathcal{Q}^2(0)}{\mathcal{E}(B_0, |2\mathbf{k}_i|) - \mu_2 \mathcal{C}(2\mathbf{k}_i)} \right) A_{\mathbf{k}_i}^4 \\
&+ \sum_{i < j \leq N} \left(\mathcal{K}(\Theta_{ij}) + \frac{1}{2} \frac{\mathcal{Q}^2(\Theta_{ij})}{\mathcal{E}(B_0, |\mathbf{k}_i + \mathbf{k}_j|) - \mu_2 \mathcal{C}(\mathbf{k}_i + \mathbf{k}_j)} \right. \\
&\left. + \frac{1}{2} \frac{\mathcal{Q}^2(\pi - \Theta_{ij})}{\mathcal{E}(B_0, |\mathbf{k}_i - \mathbf{k}_j|) - \mu_2 \mathcal{C}(\mathbf{k}_i - \mathbf{k}_j)} \right) A_{\mathbf{k}_i}^2 A_{\mathbf{k}_j}^2. \tag{34}
\end{aligned}$$

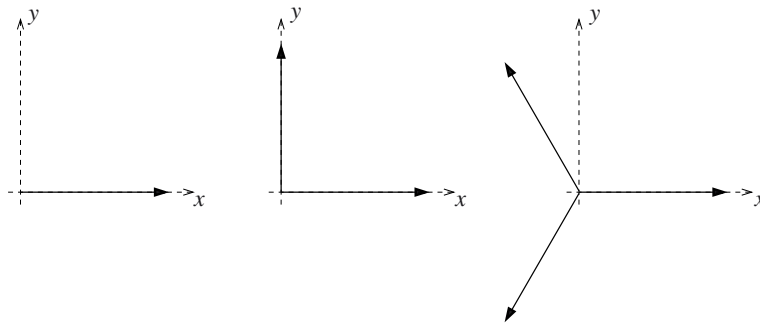


Figure 2. Sketch of the different possible regular planforms under consideration.

3. Linear stability

Being an expansion up to fourth order in the amplitudes, equation (34) contains the results we know already from the linear stability analysis [18]. Discussing the linear order in the dynamic equations corresponds to a discussion of the second order in an energy functional description. We therefore have to minimize

$$\mathcal{E}(B_0, k) - \mu_2 \mathcal{C}(\mathbf{k}_i) = \epsilon k - \frac{1}{2}(1 - k)^2 - \mu_2 k, \quad (35)$$

where $\epsilon = B_0^2/B_c^2 - 1$ is the control parameter with respect to the threshold B_c of typical ferrofluids. Determining the minimum of this expression with respect to k leads to

$$\frac{\partial}{\partial k} \left(\epsilon k - \frac{1}{2}(1 - k)^2 - \mu_2 k \right) = \epsilon - \mu_2 + (1 - k) = 0 \quad (36)$$

$$\epsilon k - \frac{1}{2}(1 - k)^2 - \mu_2 k = 0. \quad (37)$$

The first equation represents the definition of a minimum itself, while the second condition represents the exchange of stability at onset. Below threshold, the flat surface is stable with respect to a deformed one, and the energy density difference (34) is therefore negative. If the deformed surface is stable, its energy density is positive. As the solution of equations (36), (37) we find in dimensionless units

$$k = 1 \quad \text{and} \quad \epsilon = \mu_2. \quad (38)$$

This solution agrees with the findings in [18], where we could show that the characteristic wavelength at onset is not changed compared to typical ferrofluids, while the threshold itself is enhanced by the shear modulus of the medium.

4. Stability of different geometries

We discuss the stability of one of the regular patterns compared to the other ones. The specific geometries used to calculate $\mathcal{C}(\mathbf{k}_i)$ in equation (31) are illustrated in figure 2. We also assume that the magnetic field is close to the critical field, permitting us to take the wavevector to be identical to the characteristic wavevector at onset, $k = 1$.

4.1. Stripe solutions

Starting with the simplest case, we discuss the stability of stripe patterns on the surface. For convenience, we take the only wavevector appearing parallel to the x -axis, $k_i = \delta_{ix}$, and obtain

$$\mathcal{U} = -\frac{1}{2}(\epsilon - \mu_2)A^2 + \frac{1}{4}\left(\frac{5}{16} + \frac{\eta^2}{4(\epsilon - \mu_2) - 1}\right)A^4. \quad (39)$$

For simplicity, we follow [19, 20] and neglect ϵ in the denominator of the fourth-order term without any noticeable change of the results. Minimizing (39) with respect to the amplitude, we get

$$A_R = \sqrt{\frac{\epsilon - \mu_2}{\frac{5}{16} - \frac{\eta^2}{1+4\mu_2}}} \quad (40)$$

and

$$\left.\frac{\partial^2 \mathcal{U}}{\partial A^2}\right|_{A=A_R} = 2(\epsilon - \mu_2) = 0. \quad (41)$$

Thus, from this discussion we cannot draw any conclusion for the stability of stripes (as was the case for $\mu_2 = 0$ [19]).

4.2. Squares

We now start to discuss two main modes perpendicular to each other yielding a square lattice (cf figure 2). To calculate the coefficient \mathcal{C} , equation (31), without loss of generality, we take the two wavevectors to be $\mathbf{k}_1 = (1, 0)$ and $\mathbf{k}_2 = (0, 1)$ and obtain

$$\begin{aligned} \mathcal{U} = & -\frac{1}{2}(\epsilon - \mu_2)(A_1^2 + A_2^2) - \frac{1-5+16\eta^2-20\mu_2}{2 \cdot 32(1+4\mu_2)}(A_1^4 + A_2^4) \\ & + \left(-\frac{9}{16} + \frac{1}{\sqrt{2}} + \eta^2 \frac{15-13\sqrt{2}+4(-3+2\sqrt{2})\mu_2}{6-4\sqrt{2}+4\sqrt{2}\mu_2}\right)A_1^2 A_2^2, \end{aligned} \quad (42)$$

where we have again neglected ϵ in the denominator of the fourth-order terms. Minimizing equation (42) leads to the amplitude $A_S = A_S(\epsilon, \mu_2, \eta)$. Obviously, $\epsilon - \mu_2 > 0$ is a necessary condition for the stability of square solutions.

In figure 3 the value of the control parameter ϵ is plotted as a function of the magnetic susceptibility χ for $A_S = 0.25$ and different values of the shear modulus μ_2 . The isolines separate configurations in the parameter space with amplitudes smaller and higher than $A_S = 0.25$. In [20], for $\mu_2 = 0$, the plot has been used to illustrate the maximum magnetic susceptibility at which the method diverges. As can be seen in figure 3, for finite shear modulus the validity range of the method is increased to larger magnetic susceptibilities. For hexagons (cf section 4.3), a similar result is obtained.

Following the method of Gailitis [19], i.e. starting with a more general ansatz for the wavevectors that include stripes as a special case, we find that, even for $\mu_2 > 0$, stripes are always unstable with respect to squares.

4.3. Hexagons

We now discuss a regular hexagonal pattern generated by the three main wavevectors with angles of $2\pi/3$ (cf figure 2). The difference in surface energy density with respect to the flat

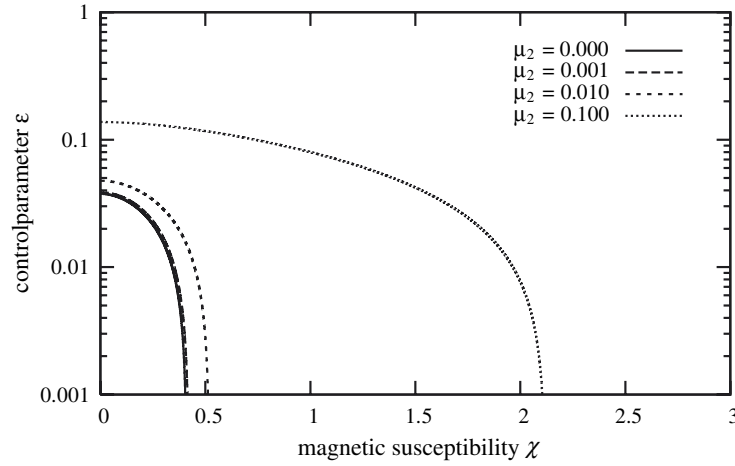


Figure 3. Isolines separating regions in the χ - ϵ -plane in which the amplitudes of squares are smaller or higher than 0.25 for different values of the elastic shear modulus μ_2 . The critical magnetic susceptibility is enhanced with higher shear modulus.

surface, equation (34), becomes

$$\begin{aligned} \mathcal{U} = & -\frac{1}{2}(\epsilon - \mu_2)(A_1^2 + A_2^2 + A_3^2) - \frac{3}{4}\eta A_1 A_2 A_3 + \frac{1}{4} \left[\frac{5}{16} - \frac{\eta^2}{1 + 4\mu_2} \right] (A_1^4 + A_2^4 + A_3^4) \\ & + \left[-\frac{15}{32} + \frac{3}{8}\sqrt{3} + \left(\frac{11}{8} - \frac{7\sqrt{3}}{8} \right) \eta^2 \right. \\ & \left. - \frac{(\frac{3}{4} - \sqrt{3})^2 \eta^2}{(1 - \sqrt{3})^2 + 2\sqrt{3}\mu_2} \right] (A_1^2 A_2^2 + A_2^2 A_3^2 + A_1^2 A_3^2). \end{aligned} \quad (43)$$

In the following, we will refer to the expressions written in the first and second square brackets as $\beta(0, \mu_2)$ and $\beta(2\pi/3, \mu_2)$, respectively, since in the limit of vanishing elasticity they are identical to those given by Gailitis [19]. For the same reason, we will also refer to $(3/4)\eta$ as γ .

We choose a regular hexagonal pattern and obtain from (43) by minimization

$$A_H = A_1 = A_2 = A_3 = \frac{\gamma \pm \sqrt{\gamma^2 + 4(\epsilon - \mu_2)[\beta(0, \mu_2) + 4\beta(2\pi/3, \mu_2)]}}{2[\beta(0, \mu_2) + 4\beta(2\pi/3, \mu_2)]}. \quad (44)$$

The hexagonal solutions exist only if the square root in equation (44) is real, and they are stable if the second derivative of equation (43) with respect to the amplitudes is negative, leading to

$$\frac{-1}{4[\beta(0, \mu_2) + 4\beta(2\pi/3, \mu_2)]} < \frac{\epsilon - \mu_2}{\gamma^2} < 2 \frac{\beta(2\pi/3, \mu_2) + \beta(0, \mu_2)}{[2\beta(2\pi/3, \mu_2) - \beta(0, \mu_2)]^2}. \quad (45)$$

Since the β -values are positive (at least for $\chi \leq 1$), hexagons can exist already below the linear threshold $\epsilon = \mu_2$. This existence range shrinks, however, for ferrogels compared to ferrofluids, since $\beta(\theta, \mu_2) > \beta(\theta, 0)$ for both $\theta = 2\pi/3$ and 0. For the same reason, the amplitude of the hexagonal pattern (44) decreases with increasing elastic modulus. Clearly, elasticity stabilizes a system against the Rosensweig instability, which is manifest not only in an increase of the (linear) threshold but also in a decrease of the spike height. The discussion for the stability boundary at high positive values of $\epsilon - \mu_2$ in equation (45) is less stringent. However, there is a strong tendency that this stability boundary is shifted to smaller values in ferrogels for realistic material parameters.

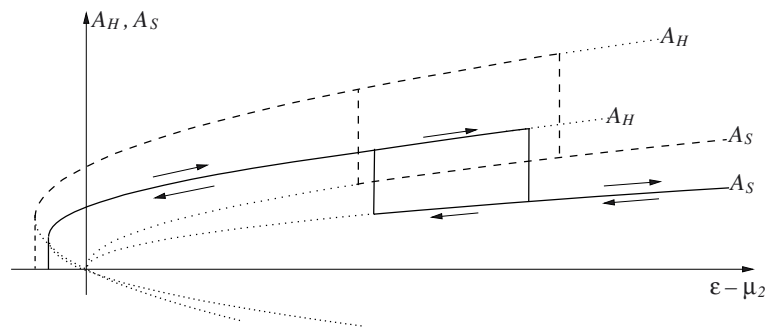


Figure 4. Qualitative sketch (not to scale) of the evolution of the amplitudes for squares (A_S) and hexagons (A_H). The dashed lines correspond to the case of a ferrofluid, while the solid lines qualitatively describe the behaviour for ferrogels with finite shear modulus μ_2 . The dotted lines represent the unstable branches.

Following the method of Gailitis superposing hexagons and squares, we investigate the relative stability of hexagons and squares. We find that squares are unstable with respect to hexagons under the condition

$$\frac{\epsilon - \mu_2}{\gamma^2} < \frac{\beta(0, \mu_2) + 2\beta(\pi/2, \mu_2)}{[2\beta(2\pi/3, \mu_2) + 2\beta(\pi/6, \mu_2) - 2\beta(\pi/2, \mu_2) - \beta(0, \mu_2)]^2}, \quad (46)$$

which is just Gailitis's expression, but with μ_2 -dependent β -abbreviations

$$\beta(\pi/2, \mu_2) = -\frac{9}{16} + \frac{1}{\sqrt{2}} + \frac{15 - 13\sqrt{2} - 4(3 - 2\sqrt{2})\mu_2}{6 - 4\sqrt{2} + 4\sqrt{2}\mu_2} \eta^2 \quad (47)$$

$$\beta(\pi/6, \mu_2) = \frac{3}{32}(4\sqrt{6} - 7) + \frac{116 - 41\sqrt{6} - (64 - 28\sqrt{6})\mu_2}{16(2 - \sqrt{6} - 2\mu_2)} \eta^2. \quad (48)$$

Figure 4 shows the evolution of the amplitudes with respect to the control parameter for zero and non-vanishing shear modulus. We note a decrease in size of the hysteretic region (for negative $\epsilon - \mu_2$) with increasing shear modulus. While in the case of no elasticity the lower boundary is at -0.25 , it is shifted to -0.24 for a shear modulus of $\mu_2 = 0.1$ (where both values are taken for a magnetic susceptibility of $\chi = 0.1$). The second hysteretic region for the transition between squares and hexagons also shrinks with increasing μ_2 . For instance, the lower boundary of the hysteresis loop at 5.7 (for the right-hand side of equation (46)) for $\mu_2 = 0$ increases to 6.9 for $\mu_2 = 0.1$, while the upper boundary of the hysteresis loop at 540 for $\mu_2 = 0$ is reduced to 480 for $\mu_2 = 0.1$ ($\chi = 0.1$). This result should be experimentally detectable, at least qualitatively.

References

- [1] Rosensweig R E 1985 *Ferrohydrodynamics* (Cambridge: Cambridge University Press)
- [2] Odenbach S 2002 *Magnetoviscous Effects in Ferrofluids* (Berlin: Springer)
- [3] Zrínyi M, Barsi L and Büki A 1996 *J. Chem. Phys.* **104** 8750
- [4] Collin D, Auernhammer G K, Gavot O, Martinoty P and Brand H R 2003 *Macromol. Rapid Commun.* **24** 737
- [5] Lenglet J, Bourdon A, Bacri J-C and Demouchy G 2002 *Phys. Rev. E* **65** 031408
- [6] Blums E 1995 *J. Magn. Magn. Mater.* **149** 111
- [7] Ryskin A, Müller H-W and Pleiner H 2003 *Phys. Rev. E* **67** 046302
- [8] Ryskin A and Pleiner H 2004 *Phys. Rev. E* **69** 046301
- [9] Ryskin A and Pleiner H 2005 *Phys. Rev. E* **71** 056303

-
- [10] Huke B, Pleiner H and Lücke M, to be published
 - [11] Pleiner H, Jarkova E, Müller H-W and Brand H R 2001 *Magnetohydrodynamics* **37** 254
 - [12] Jarkova E, Pleiner H, Müller H-W, Fink A and Brand H R 2001 *Eur. Phys. J. E* **5** 583
 - [13] Ryskin A, Pleiner H and Müller H-W 2003 *Eur. Phys. J. E* **11** 389
 - [14] Jarkova E, Pleiner H, Müller H-W and Brand H R 2003 *J. Chem. Phys.* **118** 2422
 - [15] Jarkova E, Pleiner H, Müller H-W and Brand H R 2003 *Phys. Rev. E* **68** 041706
 - [16] Bohlius S, Brand H R and Pleiner H 2004 *Phys. Rev. E* **70** 061411
 - [17] Harden J L, Pleiner H and Pincus P A 1991 *J. Chem. Phys.* **94** 5208
 - [18] Bohlius S, Brand H R and Pleiner H 2006 *Z. Phys. Chem.* **220** 97
 - [19] Gailitis A 1977 *J. Fluid Mech.* **82** 401
 - [20] Friedrichs R and Engel A 2001 *Phys. Rev. E* **64** 021406